International Journal of Structural Stability and Dynamics
Vol. 22, No. 11 (2022) 2250133 (15 pages)

DOI: 10.1142/S0219455422501334

Study on the Nonlinear Dynamic Characteristics of Spherical Rubber Isolators by Experiments and Simulations Based on Harmonic Balance Method

Hao Li[*,†], Chengliang Yang[*,‡], Shaoxin Wang[*], Ping Su[*], Youqiang Zhu[*], Xingyun Zhang[*], Zenghui Peng[*] and Quanquan Mu[*]

[*]*State Key Laboratory of Applied Optics*
Changchun Institute of Optics
Fine Mechanics and Physics
Chinese Academy of Sciences
Changchun 130033, P. R. China

[†]*Center of Materials Science and Optoelectronics Engineering*
University of Chinese Academy of Sciences
Beijing 100049, P. R. China
[‡]*chengliangyang@ciomp.ac.cn*

Received 4 March 2021
Accepted 17 March 2022
Published 20 April 2022

This study aims to elucidate the nonlinear characteristics (dynamic stiffness and damping) of a thin-walled hallowed spherical rubber isolator subjected to harmonic excitations using harmonic balance method (HBM). Firstly, harmonic excitation experiments with different loads and different acceleration levels were carried out to test the softening effect of the spherical rubber isolator. The dependence of the dynamic stiffness and damping of the spherical rubber isolator on the displacement amplitude was established. Secondly, the Nth harmonic of the experimental time signal was extracted, and the nonlinear contribution of the second and third harmonics to the experimental results was verified. Finally, the simulations were performed and the results were in line with the experimental results. Our study identifies that the nonlinear model is feasible to predict the vibration characteristic of the thin-walled hallowed spherical rubber isolation systems.

Keywords: Spherical rubber isolator; harmonic excitation; harmonic balance method (HBM); dynamic stiffness; dynamic damping; frequency response function (FRF).

1. Introduction

In recent years, rubber materials with unique mechanical properties have been widely used in various engineering fields, including space applications, sensors, bio-engineering devices, robotics, and mechanical engineering, etc. Their wide application is

[‡]Corresponding author.

due to their relative flexibility since they can withstand deformation up to several hundreds and return to their original shape after stress release. This elastic property facilitates their wide use as a flexible coupling between stiff components in various constructions. They are often used in mechanical engineering as isolators, bushings, bearings, etc. In view of the harshness of the aviation vibration environment, vibration damage to electronic equipment can be inhibited on account of the special dynamic characteristics of rubber materials. Rubber isolators also play a vital role in some special occasions where metal isolators are not applicable with nonmagnetic environments required.

However, despite the extensive use of rubber materials, knowledge about the material properties is still lacking. Since rubber materials have very complex behaviors with generally nonlinear mechanical properties, it is necessary to focus on their properties to improve performance about vibration and noise abatement. In the traditional manner, nonlinear effects of the rubber need to be avoided in its working range. However, if the effect of nonlinearity on the dynamic properties of rubber materials can be fully understood, it is possible to adopt new approaches to improving the mechanical properties of rubber materials. Sjöberg and Kari introduced a detailed explanation on the underlying physical mechanisms of the nonlinearities.[1] The properties of rubber materials mainly refer to dynamic stiffness and damping, which not only depend on the chemical composition of the rubber materials, but also on temperature, humidity, vibration frequency, and vibration amplitude. Meanwhile, the difference in rubber geometry will also exert a great impact on it. As discussed by Harris and Stevenson,[2] the nonlinearity of the material often occurs due to the properties of the elastomer itself or the influence of the geometric shape. Efforts have been devoted to the static and dynamic behaviors of the rubber isolator for a better structure design. Papoulia and Kelly designed a visco-hyperelastic rubber constitutive model to represent the finite strain response of rubbers used in the vibration isolation at low frequency.[3] Richards and Singh devised distinct experimental equipment to probe into the static and dynamic stiffness of three different rubber isolators.[4] A method of nonlinear modeling was also proposed to study the dynamic characteristics of rubber isolators by Roncen, Sinou, and Lambelin.[5] The frequency-dependence of the dynamic stiffness has been thoroughly investigated through experiment, theory analysis and numerical simulation.

At present, the research methods for the nonlinear characteristics of elastomers are mainly divided into two categories. The first type is the elastomer mechanics modeling based on physical models. The finite element discretization analysis of the structural elements of the elastomer is performed using Kelvin–Voigt or Maxwell models, fractional derivatives or Bergmodel,[6–10] etc. These methods are accurate but require highly complex structural modeling. The second type is based on experimental phenomenological modeling. The dependence of the dynamic stiffness and damping of an elastic body on the amplitude is commonly demonstrated using single-degree-of-freedom system, which is specifically expressed in the form of a polynomial

or exponential[11,12] of the relative displacement amplitude. In structural dynamics, most nonlinear formulas illustrate the relationship between dynamic stiffness and damping with the relative displacement or its derivatives. Based on harmonic experiments, Franchini *et al.* obtained the dynamic characteristics of viscoelastic materials using the method of parameter identification.[13] This work used the second approach to the structure modeling with a single-degree-of-freedom system. Firstly, a harmonic experiment was designed and conducted to present the relationship between dynamic stiffness and damping against relative displacement amplitude. The single-degree-of-freedom system was modeled, and the nonlinear characteristics of the dynamic stiffness and damping of a thin-walled hallowed spherical rubber isolator were corrected. Then, the nonlinear method was used for numerical simulation to calculate the nonlinear frequency response function (FRF) of the system. The harmonic balance method (HBM), the most widely used analysis method for nonlinear systems was applied in this study. Through the comparison of the experimental measurements and simulation results, the accuracy of system modeling was verified.

This paper is mainly divided into four parts to investigate the nonlinear dynamic characteristics of the thin-walled hallowed spherical rubber isolator by employing the methods established in Ref. 5. Firstly, the structure of the harmonic experiment was briefly introduced and the vibration test data was obtained. Secondly, the harmonic signal was studied, and the efficient filter combined with the covariance adaptive matrix algorithm was used to identify the fundamental frequency and the signal amplitudes of each time interval. The frequency response of the system was extracted from the time signal of the swept-sine experiment. Thirdly, the single-degree-of-freedom system model based on the harmonic experiment was developed, and the nonlinear vibration equation was established and solved by HBM. Finally, the results of the experimental measurement and numerical simulation were compared to verify the accuracy of nonlinear modeling.

2. Experiments

Based on the influence of the geometric shape on the nonlinear characteristics, a series of experiments were conducted to explore the dynamic stiffness and damping of the thin-walled hallowed spherical rubber isolators. Figure 1 illustrates the

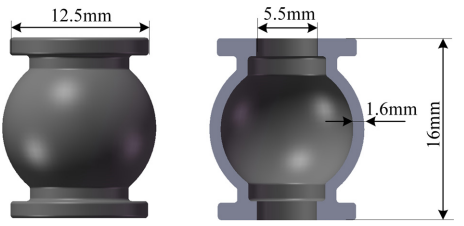

Fig. 1. Schematic diagram of the rubber isolator's structure.

schematic diagram of the rubber isolator's structure (thickness = 1.6 mm). The vibration isolator was mainly made of silicone rubbers which could be used stably at −60–+200°C over a long period of time. The range of tensile strength was 4.0–12.5 MPa.

2.1. *Experimental setup*

The structure of the system studied in this work is shown in Fig. 2. The system consists of a vibration-absorbing elastomeric material attached to an aluminum casing and a mass block. Through the cooperation of the linear bearing and the guide shaft, the movement mode of the mass block was restricted in the axial direction, thereby it could be modeled as a single-degree-of-freedom system. The entire system was fixed on the vibrator. Different harmonic excitations were applied through the vibrator to induce complex dynamic behaviors inside the spherical rubber isolator. The rotation center of the mass block was matched with that of the guide shaft to minimize the effect of tilting. Two accelerometers were installed symmetrically on the bottom of the mass block at a 180° angle to each other to detect the symmetry of the signal, ensuring that the tilted signal could be detected and corrected. The accelerometer of the input signal was installed on the top of the casing as the feedback control signal of the vibrator.

2.2. *Experimental results*

The purpose of the experiment is to characterize the nonlinear response of the system, specifically the response of the structure to different harmonic excitations. The nonlinearity of the system mainly comes from rubber materials. Firstly, the loading of the rubber isolator was investigated with a series of different loading masses [50; 60; 70; 80; 90; 100; 110; 120] g designed. After pre-experiment, the experiment was performed at room temperature with the input acceleration value set as 0.5 g and the

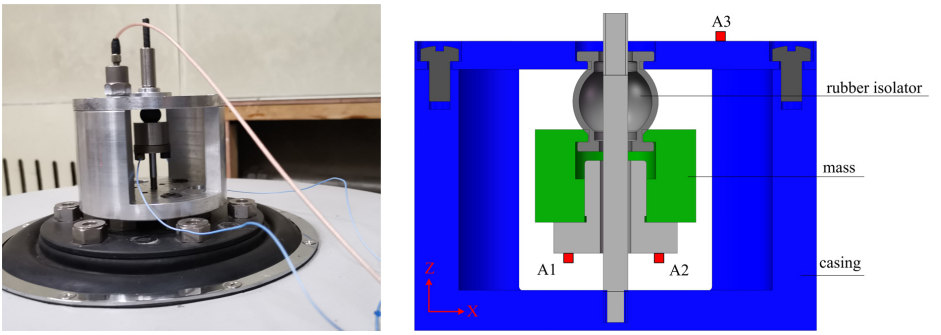

(a) (b)

Fig. 2. Experimental setups (a) photo of the structure; (b) sensor positioning diagram ($A1$, $A2$, $A3$).

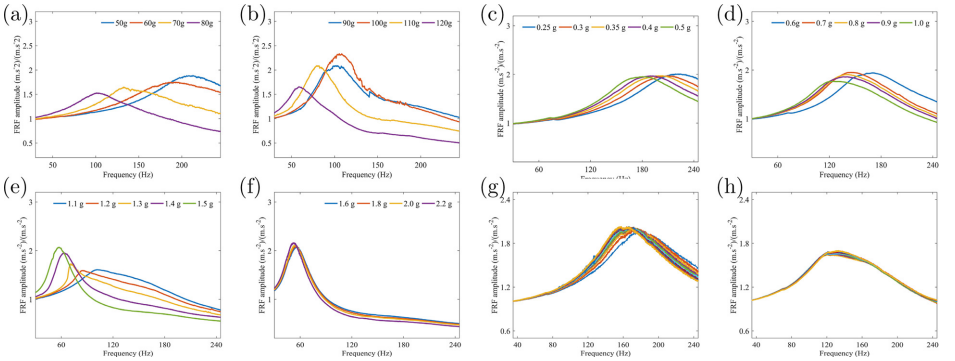

Fig. 3. Experimental FRFs for swept-sine experiments of different loads (a) and (b) and of different excitation levels (c)–(f). Repeatability for swept-sine experiments of excitation levels at 0.5 g (g) and 1.0 g (h).

frequency range set as [30; 250] Hz. The FRFs of different loads of the spherical rubber isolator under the same acceleration value were measured. FRF represents the ratio of output acceleration over input acceleration $(A1Z + A2Z)/2A3Z$. As illustrated by Figs. 3(a) and 3(b), the resonance frequency showed a downward trend as the load mass increased. The resonance peak value decreased with the increase of the load mass. Until the load mass increased to 90 g, a large nonlinear effect appeared where the resonance peak value increased to a certain value and then declined. To study the harmonic response under different excitations as well as to avoid the nonlinear influence of the load to obtain a stable response, the load mass was set as 60 g for subsequent research.

A sine frequency sweep experiment was designed and carried out at room temperature. Through the pre-experiment, the small value was densely applied and the large value was loosely applied. The input acceleration was [0.25; 0.3; 0.35; 0.4; 0.5; 0.6; 0.7; 0.8; 0.9; 1.0; 1.1; 1.2; 1.3; 1.4; 1.5;1.6; 1.8; 2.0; 2.2] g and frequency range was [30; 250] Hz. The swept rate was set as 0.5 oct/min to get stable response at the resonance peak. Figures 3(c)–3(f) shows the results of the FRF of different excitation. For the structure studied in this work, as the acceleration excitation increased, the amplitude initially decreased and then rose. Meanwhile, as the excitation increased, the resonance peak dropped from 220 Hz to 50 Hz, which was the softening effect of the elastomer material when it was deformed (i.e. Payne effect[14–16]).

Subsequently, a series of harmonic experiments were repeated at excitation levels of 0.5 and 1.0 g. The results of the FRF were shown in Figs. 3(g) and 3(h). It can be observed that for a fixed value of acceleration excitation input, the resonance peak value slowly decreased. This phenomenon corresponds to the Mullins effect.[17–19] Notably, the resonance peak after many experiments approached convergence, providing additional evidence for the nonlinear method used in this paper to restore the FRF of the spherical rubber isolators.

3. Multi-Harmonic Experimental Measurements

The vibrator is piloted with a logarithmic swept-sine signal. The response is regarded as stationary when the frequency evolved slowly enough (0.5 oct/min in the vicinity of the resonance). The frequency hardly changes in a small time slot, in which the signal could be considered as a quasi-periodic signal and expanded by Fourier series. The signal analysis[20] aims to determine the fundamental frequency and the harmonic amplitudes of both input and output signals at every instant. Extracting the harmonics of the experimental signal is mainly carried out through the following steps. Figure 4 uses the output signal as an example to illustrate the extraction of the Nth harmonic of the amplitude signal.

Firstly, the windowing step drives the frequency increment of the response curve. The temporal distance between two time slots can be directly linked to a frequency increment through the logarithmic speed of sweep. In this work, a constant distance of 0.2 s between two time slots is chosen. Adequate points are required to complete the identification but the harmonic amplitudes can be considered as constant along the sample only when the corresponding frequency length of the slot is low enough.

The second step is frequency identification and parameter optimization. The start frequency F_{beg}, stop frequency F_{end} and average frequency F_{est} are calculated for each time slot. A band-pass filter is applied to filter the signal around the estimated fundamental frequency F_{est} (generally choose $0.9F_{\text{est}}$–$1.1F_{\text{est}}$) and eliminate the higher order harmonic signals. Then a sine sweep signal P with 4 parameters is fit as function (3.1). The four parameters are the start frequency F_{beg}, the stop frequency F_{end}, the maximum amplitude A and the phase ϕ_0. Covariance adaptive matrix (CAM-ES)[21,22] is used to optimize the four parameters owing to its quick

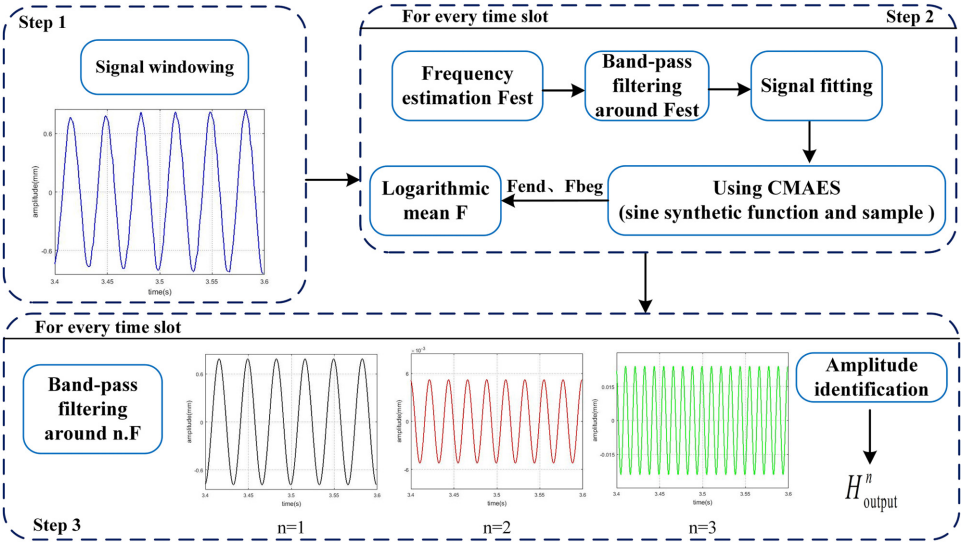

Fig. 4. Extraction of the Nth harmonic algorithm scheme.

convergence and low noise sensitivity. This algorithm can minimize the error between the sample and the synthesized signal, thereby ensuring the accuracy of the entire optimization process. The optimized fitness function is the mean square error between the synthesized signal and the sample, where amplitude A is the maximum value of the sample. Phase ϕ_0 is previously estimated by a zero-crossing scheme due to its sensitivity. The beginning of the synthetic signal is set at the first point after zero-crossing. The phase ϕ_0 is estimated by $\pm\arccos(y/A)$, where y represents the value of the first point, and the sign represents the direction of the zero-crossing. The parameters are bounded for the optimization algorithm after estimation (i.e. A, F_{beg} and $F_{\text{end}} \pm 10\%$, $\phi_0 \pm 10^\circ$). The fundamental frequency F of the sample is defined as the logarithmic mean between F_{beg} and F_{end}.

$$P = \text{Asin}\left\{2\pi\left[\left(\frac{F_{\text{end}}}{F_{\text{beg}}}\right)^{t/t_{\text{end}}} F_{\text{beg}}\right]t + \phi_0\right\}. \tag{3.1}$$

In the end, in order to get the Nth harmonic of the input and output signal, the signal is filtered by a band-pass filter around $n \cdot F$, then the two-parameter synthesis function is fit. The result of frequency identification does not need to be optimized. Only the phase and amplitude are used as the optimized quantities to obtain the Nth harmonic of the input and output signal.

Figure 5 illustrates the results of the first three harmonics extracted from the input signal and output signal, where green, blue, and red represent the first, second and third harmonics, respectively. The first harmonic signal extracted from the input signal is approximately a smooth straight line, and the first harmonic signal extracted from the output signal meets the trend of the output signal. The results indicate that the input excitation and output amplitude response of higher harmonics have nonlinear contributions. However, the contribution of the second harmonic and the third harmonic response to the overall nonlinearity are very small, both of

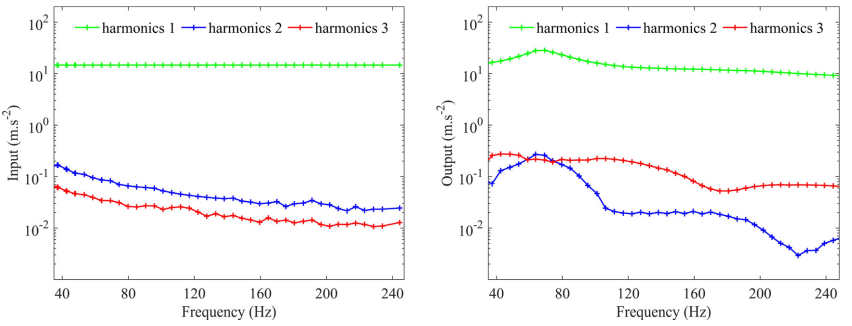

(a) (b)

Fig. 5. (Color online) Input (a) and output (b) harmonics for the experiment with a constant excitation level of 1.5 g for harmonics 1 (green), 2 (blue), and 3 (red).

which are less than 2% of the amplitude of the first harmonic. Therefore, this work does not include the contribution of higher harmonics.

4. Modeling

Prabakaran *et al.* presented several applicable damping descriptions using three different dissipation models and identified the increase of damping with the vibration amplitude for a rubber rectangular plate.[23] Stanislas *et al.* proposed a genetic algorithm to identify the nonlinear damping and stiffness of continuous structures subjected to large-amplitude vibrations and achieved good results.[24] A procedure has been presented to identify damping and stiffness coefficients of a nonlinear single-degree-of-freedom model undergoing large-amplitude vibrations under harmonic excitation by using the first harmonic of the frequency responses.[24] In this study, we perform a single-degree-of-freedom modeling for spherical rubber isolators using the HBM to predict the first harmonic of the frequency response. This work is suited to the unidirectional tensile and compression of the spherical rubber isolators. A schematic diagram of the system is shown in Fig. 6. M represents the load mass (i.e. $M = 0.06\,\text{kg}$). K and C represent the dynamic stiffness and damping of the spherical rubber isolator, respectively. Both stiffness K and damping C are functions of the displacement amplitude $\hat{X}$. $-X$ defines the relative displacement between the mass M and the base. $\hat{X}$ corresponds to the amplitude of X. Y defines the output displacement of the mass M. $q(t)$ defines the input displacement of the system. The signal measured by experiments is expressed in output displacement $Y(t)$.

For a given input acceleration excitation of the vibrator, the dynamic equation of a single-degree-of-freedom system is as follows:

$$\mathrm{M}\ddot{X}(t) + C(\hat{X})\dot{X}(t) + K(\hat{X})X(t) = -M\ddot{q}(t), \tag{4.1}$$

$q(t)$ is the input displacement of the system, the equation can be rewritten as

$$\ddot{X} + 2\omega_0\xi\dot{X} + \omega_0^2 X = -\ddot{q}, \tag{4.2}$$

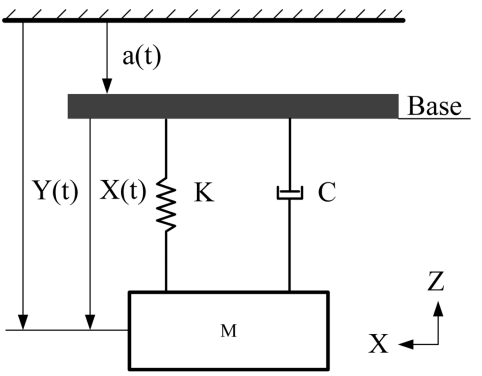

Fig. 6. Diagram of the rubber isolator modeled by a stiffness mass system.

where $\omega_0 = \sqrt{K/M}$, $\xi = C/2M\omega_0$ are, respectively, defined as the undamped circular frequency and the damping ratio.

For the supported single-degree-of-freedom system in this study, and $Y(t) = X(t) + q(t)$, the equation can be rewritten as follows:

$$\mathrm{M}\ddot{Y} + C(\dot{Y} - \dot{q}) + K(Y - q) = 0. \tag{4.3}$$

The simplified equation is as follows:

$$\ddot{Y} + 2\omega_0\xi\dot{Y} + \omega_0^2 Y = \omega_0^2 q + 2\omega_0\xi\dot{q}. \tag{4.4}$$

For the Laplace transform of the equation, the transfer function $T(\omega)$ is obtained as follows:

$$T(\omega) = \frac{1 + 2i\frac{\omega}{\omega_0}\xi}{1 - \left(\frac{\omega}{\omega_0}\right)^2 + 2i\frac{\omega}{\omega_0}\xi}. \tag{4.5}$$

By considering the above relationship, it can be obtained that when $\omega_{\max} = \omega_0\sqrt{1 - 2\xi^2}$, the amplitude of the transfer function has a maximum value $\|T(\omega)\|_{\max} \approx 1/2\xi$.

Figure 7 shows the algorithm scheme for determining the unknown function relationship between $C(\hat{X})$, $K(\hat{X})$, and $\hat{X}$. This process is based on the swept-sine experiment with different acceleration excitations, and swept rate is 0.5 (oct/min). Since the frequency changes very slowly, the response of the system can be regarded as $X(t) = \hat{X}\sin(\omega \cdot t)$.

The FRF corresponding to a given acceleration excitation can be obtained through the harmonic experiment. The maximum amplitude $\hat{X}_{\max}$ is determined by FRF, and $\hat{X}_{\max} = \|T(\omega)\|_{\max} \approx 1/2\xi$ is used to calculate the damping ratio ξ. The undamped circular frequency ω_0 is calculated through $\omega_0 = \omega_{\max}/\sqrt{1 - 2\xi^2}$. From $\omega_0 = \sqrt{K/M}$, $\xi = C/2M\omega_0$, the damping and stiffness under a given acceleration excitation can be obtained. By conducting different excitation harmonic experiments, multiple points corresponding to the dynamic stiffness $K(\hat{X})$, dynamic

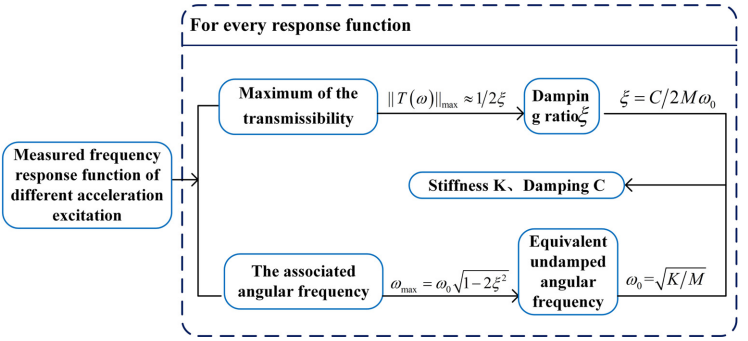

Fig. 7. Stiffness and damping algorithm scheme.

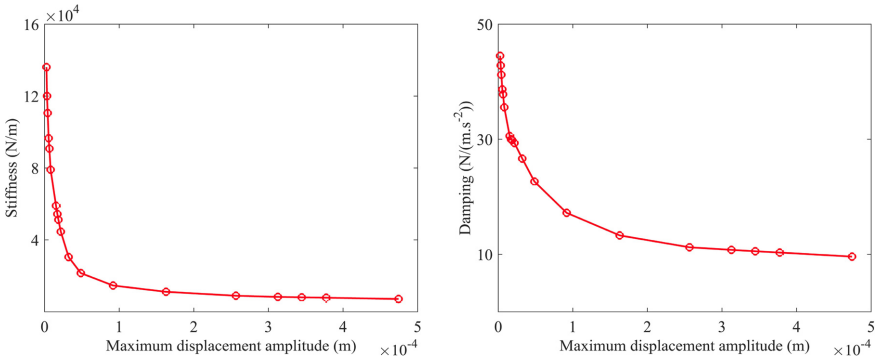

(a) (b)

Fig. 8. Evolution of the stiffness (a) and damping (b) with respect to the displacement amplitude.

damping $C(\hat{X})$ and the maximum amplitude $\hat{X}_{\max}$ can be obtained. The stiffness K and damping C of the rubber elastomer are defined as continuous functions of $\hat{X}_{\max}$ by a spline interpolation as shown in Fig. 8.

Notably, the acquired functions are established on the basis of the variable $\hat{X}_{\max}$ at the resonance frequency and the stiffness K and damping C only depend on the displacement amplitude $\hat{X}$. Hence, it is postulated that the identified values of K and C are solid as a function of the displacement amplitude. A simplified modeling of the elastomer is used by means of a reduced number of experiments.

5. Simulation

Various methods have been established to analyze the nonlinear frequency response by numerical simulation. This work mainly employs the HBM for nonlinear systems. Its fundamental principle is to express each state variable of the dynamic equation with a Fourier series to satisfy its periodicity. It is required to optimize the coefficients of the Fourier series so that the system equation has the smallest error. Marco *et al.* introduced the first-order HBM to demonstrate the nonlinear damping in large-amplitude vibrations and proved that the approach is valid for continuous systems discretized with a single-degree-of-freedom.[25] Subsequently, the third-order HBM is introduced and the equation of motion is obtained in differential form for the first time, extending the research approaches of complex nonlinear dynamics and contributes to future engineering applications.[26] This work uses HBM to solve the nonlinear problems defined by the following equations of motion:

$$M\ddot{X} + C_{NL}\dot{X} + K_{NL}X = F(t). \tag{5.1}$$

After introducing the nonlinear force, the equation can be rewritten into the following form. $F(t)$ and $F_{NL}(X)$ represent the linear and nonlinear terms of the equation, respectively.

$$M\ddot{X}(t) = F(t) + F_{NL}(X), \tag{5.2}$$

where

$$F_{NL}(X) = -C_{NL}\dot{X}(t) - K_{NL}X(t), \tag{5.3}$$

where K_{NL} and C_{NL} correspond to the nonlinear dependency of the stiffness K and the damping C with regard to the displacement amplitude $\hat{X}$.

To find the solution of the equation $X(t)$ with a specific period, $\Omega = 2\pi\omega$ is chosen to be the fundamental pulsation. As for swept-sine simulations, Ω represents the current pulsation of the excitation. The stationary solution is approximated by the truncated Fourier series with Ω as fundamental frequency such as

$$X(t) = B_0 + \sum_{k=1}^{p}(B_K \cos(k\Omega t) + A_K \sin(k\Omega t)). \tag{5.4}$$

$\{B_0, [A_K, B_K]_{K\in 1:p}\}$ is the Fourier coefficient of solution $X(t)$. Nonlinear force $F_{NL}(X)$ and excitation force $F(t)$ can also be approximated by a finite Fourier series.

$$F_{NL}(t) = C_0 + \sum_{k=1}^{p}(C_K \cos(k\Omega t) + S_K \sin(k\Omega t)), \tag{5.5}$$

$$F(t) = \sum_{k=1}^{p}(C_{K,\mathrm{ex}} \cos(k\Omega t) + S_{K,\mathrm{ex}} \sin(k\Omega t)). \tag{5.6}$$

$\{C_0, [C_K, S_K]_{K\in 1:p}\}$ and $\{[C_{K,\mathrm{ex}}, S_{K,\mathrm{ex}}]_{K\in 1:p}\}$ are the Fourier coefficients of the nonlinear force $F_{NL}(X)$ and the excitation $F(t)$, respectively. The order of the truncated Fourier series, denoted p in previous equations, is chosen in accordance with the number of significant harmonics required in the dynamical response. For the swept-sine experiments, the hypothesis made in Sec. 3 restricts the study to the first harmonic of the response, thus, $p = 1$. Afterwards the amplitude of the response is given by

$$\hat{X}(t) = \sqrt{A_1^2 + B_1^2}. \tag{5.7}$$

Equation (5.1) can be rewritten in the Fourier basis

$$\begin{bmatrix} -(\mathrm{k}\Omega)^2 M & 0 \\ 0 & -(\mathrm{k}\Omega)^2 M \end{bmatrix} \begin{bmatrix} A_K \\ B_K \end{bmatrix} = \begin{bmatrix} S_K \\ C_K \end{bmatrix} + \begin{bmatrix} S_{K,ex} \\ C_{K,ex} \end{bmatrix}. \tag{5.8}$$

The coefficients $\{C_0, [C_K, S_K]_{K\in 1:p}\}$ depend on the coefficients $\{B_0, [A_K, B_K]_{K\in 1:p}\}$. Both are calculated via the classical alternate frequency time domain method (AFT-method).[27] Thus, the following process is employed and implemented:

The nonlinear equations can be solved by calculating the relationship between $\{B_0, [A_K, B_K]_{K\in 1:p}\}$ and $\{C_0, [C_K, S_K]_{K\in 1:p}\}$. As shown in Fig. 9, $\hat{X}(t)$ can be obtained by two methods. Notably, the process can be simplified in the swept-sine experiments where the response $\hat{X}(t)$ is a sine with $p = 1$. In this case, the amplitude

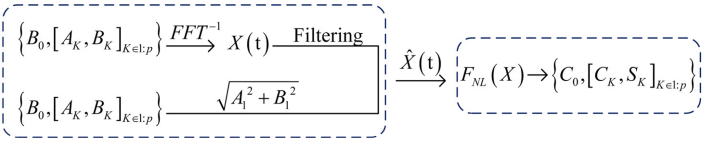

Fig. 9. AFT algorithm scheme.

of $\hat{X}(t)$ is obtained from Eq. (5.3), and AFT is no longer needed.

$$C_1 = -C_{NL}A_1\Omega - K_{NL}B_1, \tag{5.9}$$

$$S_1 = C_{NL}B_1\Omega - K_{NL}A_1. \tag{5.10}$$

Equation (5.1) can be rewritten in the Fourier basis

$$\begin{bmatrix} K_{NL}-\Omega^2 M & -C_{NL}\Omega \\ C_{NL}\Omega & K_{NL}-\Omega^2 M \end{bmatrix} \begin{bmatrix} A_1 \\ B_1 \end{bmatrix} = \begin{bmatrix} S_{1,ex} \\ C_{1,ex} \end{bmatrix}. \tag{5.11}$$

The following equation can be obtained by combining Eqs. (5.9)–(5.11):

$$\hat{X}(t)\sqrt{(C_{NL}\Omega)^2+(K_{NL}-\Omega^2 M)^2} - \sqrt{(S_{1,\mathrm{ex}})^2+(C_{1,\mathrm{ex}})^2} = 0. \tag{5.12}$$

This relationship between $\{C_0,[C_K,S_K]_{K\in 1:p}\}$ and $\hat{X}(t)$ facilitates the solving of the nonlinear problem (Eq. (5.8)) which is referred to as $H(\hat{X}(t),\Omega)=0$.

By solving the nonlinear equation, the FRF can be obtained. As for the mechanical system subjected to swept-sine excitations, a Newton–Raphson continuation method is applied with the frequency Ω and the Fourier coefficients $\hat{X}(t)$ considered as variables. The precision of system modeling is identified by comparing experimental measurement and simulation results.

6. Results and Discussion

The calculation results of the nonlinear vibrations of the thin-walled hallowed spherical rubber isolator subjected to harmonic excitations are compared with the swept-sine experiments to verify the effectiveness of the nonlinear modeling. Figure 10 illustrates the comparisons of simulation results and experimental measurements at excitation levels of [0.3; 0.4; 0.5; 0.6; 0.7; 0.8] g, in which blue dots represent experimental results and red dots represent numerical simulation results. For the simulation results of different excitations, we can obtain the softening effect, resonance peak value and resonance frequency of the spherical rubber isolator. These parameters give us a better understanding of the characteristics of such kind of spherical rubber isolator and provide additional support for rubber materials used as isolators in engineering.

However, two main deviations can be seen in the comparisons. Firstly, the calculated FRF under high excitation level is slightly different from the experimental measurement. As the acceleration excitation level increases, the

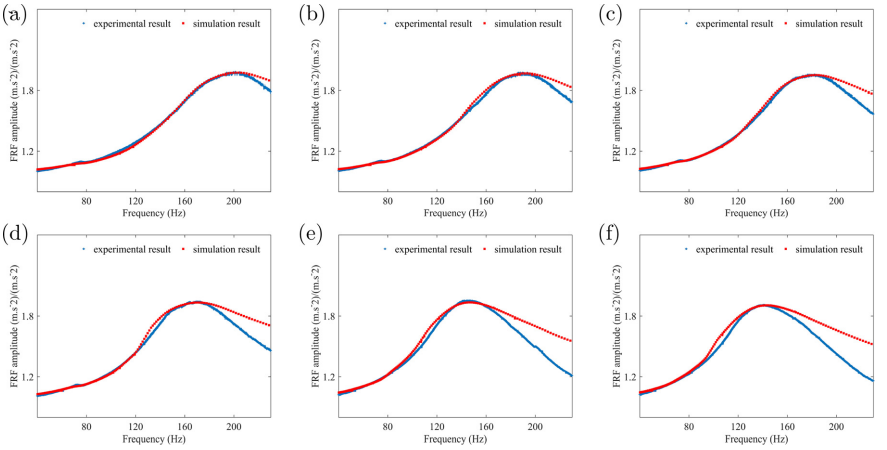

Fig. 10. (Color online) Experimental FRFs for swept-sine experiments (blue) and HBM simulations (red).

deviations become obvious. During the experiment, for high excitation levels, the temperature increases significantly, which can be attributed to the thermal effect of the elastomer. Secondly, the simulation results agree very well with the experimental results before the resonance peak, while variances appear after the resonance peak. For different acceleration excitations, the calculated FRF basically shows the same characteristics. As the frequency increases, the deviation of the acceleration value becomes larger. This shift is mainly due to the changes of rubber itself caused by resonance damage.

In spite of the deviations of FRF after the resonance peak, the modeling of the elastomer is reliable enough to capture the resonance peak, the softening effect as well as the general form of the nonlinear response for all excitation levels. It ensures the accuracy of the modeling and the effectiveness of the parameter identification, predicting the vibration characteristic of the thin-walled hallowed spherical isolation systems and providing additional supports for isolation system design.

7. Conclusions

The nonlinear characteristics of a thin-walled hallowed spherical rubber isolator subjected to harmonic excitation are studied in this work. Through swept-sine experiments, the nonlinear dynamic characteristics of spherical rubber isolators are observed, and elastomer modeling is performed. The frequency response curve is predicted by HBM method and the simulation results agree well with the experimental results, especially for the resonance frequency, resonance peak value and softening effect. The data obtained in this work provide reference for future design in damping systems with thin-walled hallowed spherical rubber isolators. These methods are conducive for practical applications of rubber damping system in engineering.

Acknowledgments

This work is supported by CAS Interdisciplinary Innovation Team and Youth Innovation Promotion Association CAS. National Natural Science Foundation of China (Grant Nos. 11774342 and 61805238), the Foundation of State Key Laboratory of Applied Optics.

References

1. M. Sjöberg and L. Kari, Testing of nonlinear interaction effects of sinusoidal and noise excitation on rubber isolator stiffness, *Polym. Test.* **22**(3) (2003) 343–351.
2. J. Harris and A. Stevenson, On the role of nonlinearity in the dynamic behaviour of rubber components, *Rubber Chem. Technol.* **59**(5) (1986) 740–764.
3. K. D. Papoulia and J. M. Kelly, Visco-hyperelastic model for filled rubbers used in vibration isolation, *J. Eng. Mater. Technol.* **119** (1997) 292–297.
4. C. M. Richards and R. Singh, Characterization of rubber isolator nonlinearities in the context of single- and multi-degree-of-freedom experimental systems, *J. Sound Vib.* **247** (2001) 807–834.
5. T. Roncen, J.-J. Sinou and J. P. Lambelin, Experiments and nonlinear simulations of a rubber isolator subjected to harmonic and random vibrations, *J. Sound Vib.* **451** (2019) 71–83.
6. N. Gil-Negrete, J. Viñolas and L. Kari, A simplified methodology to predict the dynamic stiffness of carbon-black filled rubber isolators using a finite element code, *J. Sound Vib.* **296** (2006) 757–776.
7. R. Lewandowski and B. Chorążyczewski, Identification of the parameters of the Kelvin–Voigt and the Maxwell fractional models, used to modeling of viscoelastic dampers, *Comput. Struct.* **88** (2010) 1–17.
8. M. M. Sjberg and L. Kari, Non-linear behavior of a rubber isolator system using fractional derivatives, *Veh. Syst. Dyn.* **37** (2002) 217–236.
9. M. Berg, A non-linear rubber spring model for rail vehicle dynamics analysis, *Veh. Syst. Dyn.* **30** (1998) 197–212.
10. T. H. Zhang and W. Wang, Finite element analysis of the crack behavior of rubber material, in *2nd Annual Int. Workshop on Materials Science and Engineering*, 12–14 August 2016, Guangzhou, China, pp. 723–728.
11. C. Xueqian and S. Zhanpeng, Influence of uncertainty and excitation amplitude on the vibration characteristics of rubber isolators, *J. Sound Vib.* **377** (2016) 216–225.
12. D. W. Sun and Z. G. Chen, Modelling and parameter identification of amplitude- and frequency-dependent rubber isolator, *J. Cent. South Univ. Technol.* **18** (2011) 672–678.
13. G. Franchini, I. D. Breslavsky, G. A. Holzapfel and M. Amabili, Viscoelastic characterization of human descending thoracic aortas under cyclic load, *Acta Biomater.* **130** (2021) 291–307.
14. D. Ponnamma and K. K. Sadasivuni, Interrelated shape memory and Payne effect in polyurethane/graphene oxide nanocomposites, *RSC Adv.* **3** (2013) 16068–16079.
15. X. Wang, Similarity between the damping function and Payne effect in particle-filled elastomers, in *APS Meeting*, 13–17 March 2017, New Orleans, Louisiana.
16. A. Zhao *et al.*, Insights into the Payne effect of carbon black filled styrene-butadiene rubber compounds, *Chin. J. Polym. Sci.* **39** (2021) 81–90.
17. J. Diani and B. Fayolle, A review on the Mullins effect, *Eur. Polym. J.* **45** (2009) 601–612.

18. F. Bueche, Mullins effect and rubber-filler interaction, *J. Appl. Polym. Sci.* **5** (2010) 271–281.
19. L. Mullins, Softening of rubber by deformation, *Rubber Chem. Technol.* **42** (2012) 339–362.
20. M. Claeys, J. J. Sinou and J. P. Lambelin, Multi-harmonic measurements and numerical simulations of nonlinear vibrations of a beam with non-ideal boundary conditions, *Commun. Nonlinear Sci. Numer. Simul.* **19** (2014) 4196–4212.
21. L. Azrar and R. Benamar, Semi-analytical approach to the non-liner dynamic response problem of *s–s* and *c–c* beams at large vibration amplitudes part I: General theory and application to the single mode approach to free and forced vibration analysis, *J. Sound Vib.* **224** (1999) 183–207.
22. N. Hansen and A. Ostermeier, Completely derandomized self-adaptation in evolution strategies, *Evol. Comput.* **9** (2001) 159–195.
23. P. Balasubramanian, G. Ferrari and M. Amabili, Identification of the viscoelastic response and nonlinear damping of a rubber plate in nonlinear vibration regime, *Mech. Syst. Signal Process.* **111** (2018) 376–398.
24. S. Le Guisquet and M. Amabili, Identification by means of a genetic algorithm of nonlinear damping and stiffness of continuous structures subjected to large-amplitude vibrations. Part I: Single-degree-of-freedom responses, *Mech. Syst. Signal Process.* **153** (2021) 291–307.
25. M. Amabili, Nonlinear damping in large-amplitude vibrations: Modelling and experiments, *Nonlinear Dyn.* **93** (2017) 5–18.
26. M. Amabili, Derivation of nonlinear damping from viscoelasticity in case of nonlinear vibrations, *Nonlinear Dyn.* **97** (2018) 1785–1797.
27. T. M. Cameron and J. H. Griffin, An alternating frequency/time domain method for calculating the steady-state response of nonlinear dynamic systems, *J. Appl. Mech.* **56** (1989) 149–154.